Journal of Solid State Chemistry **148,** 278–285 (1999)
Article ID jssc.1999.8448, available online at http://www.idealibrary.com on IDEAL®

Possible 3D Carbon Structures as Progressive Intermediates in Graphite to Diamond Phase Transition

José Fayos

Departamento de Cristalografía, Instituto Rocasolano (CSIC), Serrano 119, Madrid-28006, Spain

Received January 28, 1999; in revised form July 7, 1999; accepted July 22, 1999

Modeling successive contractions of conventional graphite structure in different directions, together with some chemical reactions (consisting of Csp^2 to Csp^3 hybridization changes, followed by new bonding between closing carbons), simulates a graphite to diamond phase transition. The stable intermediate structures were optimized by a molecular mechanic approach, giving rise to new hypothetical 3D crystal structures which progress along the transition in the order of increasing density from 2.22 to 3.30 gcm^{-3}. There are graphite bilayers with planar and pyramidal Csp^2, graphite bilayers with Csp^2 and Csp^3, diamonds with Csp^2 and Csp^3, and diamonds with only Csp^3. We present eight different models: seven orthorhombic and one cubic *Ia*-3, the latter close to one structure proposed for supercubane C8. Additionally, some other noncrystalline models, made by optimizing unconstrained clusters from the above crystal models, are proposed. Although these structures are speculative, some of them present synthetic polycrystal X-ray diffraction with their highest peaks among those observed in reported experimental phases between graphite and diamond, which gives more reality to the proposed models. © 1999 Academic Press

Key Words: **carbon; structure; graphite; diamond; interphases; phase transition; modeling.**

INTRODUCTION

There are two known three-dimensional (3D) allotrope forms of carbon, diamond (Csp^3 with density $d = 3.52\ gcm^{-3}$) and graphite (Csp^2, $d = 2.27\ gcm^{-3}$), the first with cubic and hexagonal structural modifications and the second with hexagonal and rhombohedral modifications (1). Although less known, there is another 3D superdense modification, C8 (Csp^3, $d = 4.1\ gcm^{-3}$), found in condensed carbon films (2) whose structure was later revised (3). Additionally, other structures present in carbon films have been reported, some of them hydrogenated and many other amorphous and with Csp^3:Csp^2 mixture (4, 5). In some amorphous carbons (a-c here after), a proportion of 50% Csp^3:Csp^2 has been detected by NMR (6); moreover, this proportion could be controlled by the sputtering powder in ion beam experiments and analyzed by measurements of the complex dielectric function (7). These experiments show that a-c films are representative of a metastable phase of carbon having properties of both allotropes: diamond and graphite. X-ray powder analysis also suggests the presence of both Csp^3 and Csp^2 in a-c films prepared by the glow discharge technique (8), as it has film appearance and electrical properties of graphite, but has no X-ray peaks for $d > 2$ Å as in diamond. There is also evidence by electron microscopy (9) that diamond nucleation from the gas phase proceeds through a graphitic intermediate. It has been observed a metastable diamond and suggested to be a metastable graphite, as interphases in the transition graphite-diamond (10), or it has been suggested that anisotropic diamond crystals form interstellar dust (11), these materials being perhaps similar to the above structures found in carbon films. Nevertheless, we did not find the proposed structures for any of the above experimentally observed intermediate phases.

On the other hand, some theoretical structures have been proposed for new carbon allotropes (12). As we are interested in this work on 3D structures, we should mention some of the more characteristic ones among them. First, a 3D model of Csp^2 which forms a metallic net of polyene chains running along two dimensions, with no conjugation in the third dimension (13). This is a ThSi structure type, proposed as a possible interphase between graphite and diamond ($d = 2.97\ gcm^{-3}$, C–C = 1.44 Å and a *formation energy* per atom with respect to graphite of $\Delta E_{gra} = 17.1$ Kcal/mol.at), which forms rings of 10 and 12 carbons, and another similar model mixing Csp^2 with Csp (14). Second, the graphyne model (15), which has the same planar symmetry of graphite but replaces 1/3 of Csp^2 by Csp. This would make bigger the largest void in graphite (taking $R_{VDW}C = 1.7$ Å) from 0.52 to 0.98 Å, allowing Li^+($R = 0.6$ Å) and Na^+($R = 0.95$ Å) to be incorporated without increasing interlayer separation. Third, some proposed 3D Csp^2 graphite foams (16) of low density, $d = 1$ to $2.3\ gcm^{-3}$ and $\Delta E_{gra} = 2.3$ to 13.9 Kcal/mol.at.

However, taking into account the experimental evidence of Csp^3–Csp^2 mixing in carbon films, the next two

0022-4596/99 $30.00

structures are of special significance. The first one is a 3D net where parallel two dimensional nets of Csp^2 are connected by approaching part of the structure in a layer toward the next layer (17). Then, 3D Csp^3–Csp^2 *terrace* layer nets are formed with intermediate density between diamond and graphite ($d \approx 3.0\ \mathrm{gcm}^{-3}$, $\Delta E_{\mathrm{gra}} = 19.9$–$29.3$ Kcal/mol.at) and close interlayer distances of $\cong 2.4$ Å (allowing metallic properties). The second is a 3D model where parallel triptycyl moieties are linked by fused benzene rings (18), forming hexagonal, Kagome-type crystal structures with Csp^3 and Csp^2. These structures have large empty channels between benzene rings, densities in the range $d = 1.05$ to $2.21\ \mathrm{gcm}^{-3}$, and a stability close to that of diamond ($\Delta E_{\mathrm{gra}} = 6.0$ to 10.9 Kcal/mol.at).

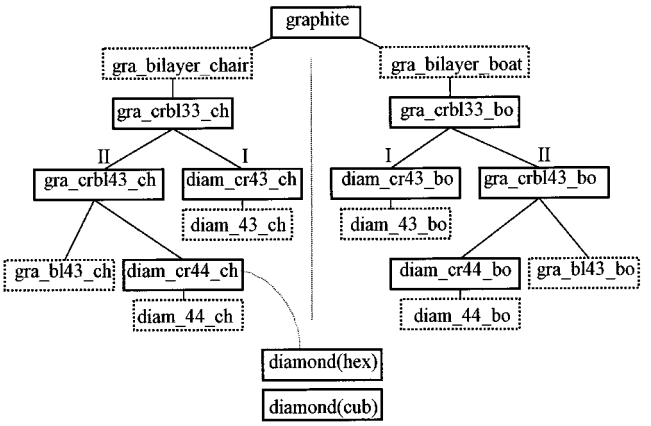

FIG. 1. A genealogical tree representing the proposed phases between graphite and diamond. Continuous squares are for crystalline phases, while discontinuous are for non crystalline clusters. The connecting lines represent possible transitions.

MODELING

We suggest in this work a continuous model for the structural phase transition from graphite to diamond. Along this transition, some stable theoretical carbon structures are generated, which are related as progressive structural modifications. Most of these structures are new and a few are related to some previously reported structures. The transition is divided into several steps, assuming successive contractions of graphite structure in different directions. For each contraction, some carbon atoms become neighbors and we create new bonds in between, we change carbon hybridization if it is necessary, and, sometimes, we also break some bonds. It is assumed, although not included in any calculation, that it should be high temperature to allow the above chemical process in a real experiment. After this speculative process, the new structures created are optimized by a molecular mechanic (MM) approach (19), giving rise to our proposed intermediate phases between graphite and diamond. Along the transition steps, we will account for the metastable crystalline and noncrystalline structures which, together with the deformation trajectories, are shown in the genealogical tree of Fig. 1. The potential terms minimized in the MM optimization are those of a Dreiding II force field (19), that is $E_{\mathrm{tot}} = E_{\mathrm{bon}} + E_{\mathrm{ang}} + E_{\mathrm{tor}} + E_{\mathrm{inv}} + E_{\mathrm{VDW}}$, accounting each term for the molecular geometry deviations from the expected geometry for structures made of Csp^2 and Csp^3. The terms being $E_{\mathrm{bon}} = 1/2K_{\mathrm{b}}(R - R_{\mathrm{o}})^2$ and $E_{\mathrm{ang}} = 1/2(\cos\omega - \cos\omega_{\mathrm{o}})^2\, K_\theta/\sin 2\omega_{\mathrm{o}}$ (R_{o} and ω_{o} are the expected bond length and angle); $E_{\mathrm{tor}} = \sum_{n=1}^{6} 1/2K_{\theta,n}(1 - d\cos(n\theta))$ ($d = 1$ when *cis* conformation is the minimum and $d = -1$ when it is the maximum); $E_{\mathrm{inv}} = \langle 1/2(\cos\omega - \cos\omega_{\mathrm{o}})^2 K_\omega/\sin^2\omega_{\mathrm{o}}\rangle$ (for an umbrella nonplanar group of four atoms with only three bonds, the average is over their three individual out-of-plane angles, where ω_{o} are the individual out-of-plane best angles); and $E_{\mathrm{VDW}} = D_{\mathrm{o}}[(R_{\mathrm{o}}/R)^{12} - 2(R_{\mathrm{o}}/R)^6]$ (accounting for Van der Waals forces). Table 1 shows the space group, cell dimensions, density, and atomic positions for the proposed crystal structures and also for the conventional graphite and diamond (ICSD: Inorganic Crystal Structure Database). The geometry of these models and partial energies after their minimization are shown in Table 2. The proposed phase transition mechanisms are described below.

Figure 2a shows the structure of graphite, with its Csp^2 stacked in five layers along the hexagonal *c*-axis; it is the graph_cluster in Table 2. By compression in the *c* direction (and assuming high temperature) the structure might break some bonds (those crossed by fine lines) and new bonds can be made between closing layers, so as to isolate just strips of fused benzene rings on each layer. Figures 2b and 2c show two mechanisms for making new bonds, the first deforming planar benzene rings toward chairs (ch) and the second deforming them toward boats (bo); in both cases a new type of layers, let us say *bilayers*, are formed along the *b*-axis. Figures 2b and 2c show just one bilayer before optimization. These structures stabilize (optimize) into models gra_bl_chair and gra_bl_boat, described in Table 2. Both bilayers are about 3 Å thick and they present rings of 10, 8, and 6 carbons, the latter two being chairs in the first structure and boats in the second. In both structures there are two types of Csp^2, one planar C2 and another pyramidal C1 (see Fig. 3a), the latter responsible for the higher energies with respect to graphite.

The crystal packing of the bilayers with chair conformation can be described by the structure gra_crbl33_ch, where 33 means that both independent carbons C1 and C2 have three connections. Two bilayers are shown in Fig. 3a while Fig. 3b shows only one bilayer viewed along the *c*-axis. The structure optimization leads to an orthorhombic cell with symmetry *Cmma*. Confirmation of *Cmma* as the best space group was done by relaxing the crystal structure symmetry to *P*1, then optimizing all atomic positions (which were all

TABLE 1
Crystal Data for the Proposed Crystalline Models and Other Known Phases of Carbon: Space Group, Unit Cell in Å, and Calculated Density in gcm^{-3}

Phase	Space group	Unit cell			Dens	*m*	*sym*	*x*	*y*	*z*	*m*	*sym*	*x*	*y*	*z*
graphite	$P6_3mc$	2.461	—	6.708	2.267	2*a*	3m.	0	0	0	2*b*	3m.	1/3	2/3	0.0050
gra_crbl33_ch	*Cmma*	4.575	5.304	5.635	2.334	8*m*	m..	0	0.1104	0.2371	8*l*	..2	1/4	0	0.1275
gra_crbl33_bo	*Cmmm*	4.525	5.334	5.925	2.222	8*n*	m..	0	0.1382	0.2303	8m	..2	1/4	0	0.1230
gra_crbl43_ch	*Pcca*	4.700	5.978	4.448	2.554	8*f*	1	0.3613	0.2469	0.1589	8*f*	1	0.1614	0.1297	0.3357
gra_crbl43_bo	*Pban*	4.048	4.885	6.495	2.484	8*m*	1	0.0460	0.1352	0.2528	8m	1	0.3379	0.1653	0.1417
diam_cr43_ch	*Cmma*	4.964	5.163	4.387	2.839	8*m*	m..	0	0.0855	0.3443	8*l*	..2	1/4	0	0.1699
diam_cr43_bo	*Cmmm*	4.870	5.565	4.406	2.673	8*n*	m..	0	0.1420	0.3260	8m	..2	1/4	0	0.1704
diam_cr44_bo	*Pban*	4.127	4.937	4.819	3.250	8*m*	1	0.0257	0.1387	0.3376	8m	1	0.3312	0.1644	0.1871
diam_cr44_ch	*Ia*-3	4.591	—	—	3.297	16*c*	.3.	0.1625	0.1625	0.1625					
diam_cr44_ch*	*Ia*-3	4.261	—	—	4.124	16*c*	.3.	0.1567	0.1567	0.1567					
BC-8	*Ia*-3	4.293	—	—	4.03	16*c*	.3.	0.1464	0.1464	0.1464					
supercubane	*Im*-3	4.28	—	—	4.1	16*f*	.3.	0.1666	0.1666	0.1666					
diamond (hex)	$P6_3/mmc$	2.52	—	4.12	3.521	4*f*	3m.	1/3	2/3	0.0625					
diamond (cub)	*Fd*-3*m*	3.567	—	—	3.516	8*a*	-43m	0	0	0					

Note. Atomic positions are shown by their multiplicity (*m*), site symmetry (*sym*), and fractional coordinates of independent atoms.

free), and finally checking which space group better described the new structure. We found that it was indeed *Cmma*, the real symmetry in the assumed *P*1 cell with a tolerance of 0.1 Å. As a second test, we broke also the translational order by taking a *P*1 triclinic cell of dimensions $3a \times 3b \times c$; the optimization of the 144 totally inde-

TABLE 2
Partial and Total Molecular Mechanic Energy per Atom (see text), in Kcal/mol.at, for All Minimized Structures, Followed by Their Characteristic Structural Geometry

Phase	E_{bon}	E_{ang}	E_{tor}	E_{inv}	E_{vdw}	E_{tot}	C…C	C12	C11	α_{op}	α_{con}	C22	α_{op}	α_{con}
graphite	1.23	0	0.14	0.02	1.14	2.52	3.35		1.42	120				
gra_crbl33_ch	2.57	5.88	27.49	1.02	5.35	42.30	3.19	1.43	1.48	107	114	1.44	129	116
gra_crbl33_bo	2.88	5.96	23.09	1.06	6.20	39.18	3.22	1.43	1.48	105	115	1.46	127	116
gra_crbl43_ch	12.23	9.75	2.50	1.14	10.22	35.83	3.20	1.60	1.54	(104 –	122)	1.76	(98 –	115)
gra_crbl43_bo	64.91	12.68	2.26	1.28	25.08	106.20	3.23	1.39	1.37	(100 –	119)	2.14	(100 –	120)
diam_cr43_ch	4.58	3.46	2.58	0	6.13	16.76	1.63	1.52	1.70	(105 –	123)	1.49	120	120
diam_cr43_bo	0.93	9.87	2.12	0	1.70	14.62	1.53	1.52	1.58	(90 –	117)	1.50	126	117
diam_cr44_bo	67.36	25.53	2.15	–	25.30	120.34	1.58	1.46	1.39	(90 –	127)	2.10	(99 –	121)
diam_cr44_ch	19.73	6.09	2.70	–	15.61	44.13		1.39	1.69	104	114			
diam_cr44_ch*	4.09	10.47	3.48	–	(0)	17.18		1.38	1.55	102	116			
BC-8	0.48	20.72	2.36	–	92.66	116.22		1.54	1.54	98	118			
supercubane	17.56	61.68	2.62	–	13.19	95.05		1.24	1.43	90	125			
diamond(hex)	0.62	0	1.06	–	7.93	9.61			1.54	109				
diamond(cub)	0.65	0	0	–	4.69	5.34			1.54	109				
graph_cluster	0.97	0	0.09	0.01	4.38	5.45	3.35		1.42	120				
gra_bl_chair	1.91	3.47	20.38	0.72	4.97	31.44		1.44	1.50	107	115	1.43	130	115
gra_bl_boat	2.20	3.67	17.5	0.74	5.55	29.69		1.44	1.49	105	115	1.45	128	116
gra_bl43_ch	10.38	8.83	2.18	0.91	9.69	32.00		1.41	1.55	(104 –	122)	1.76	(97 –	115)
gra_bl43_bo	47.65	13.08	1.91	0.98	21.19	84.83		1.40	1.37	(109 –	119)	2.13	(100 –	120)
diam_43_ch	3.14	3.03	2.22	0.07	5.02	13.42	1.63	1.52	1.71	(105 –	123)	1.49	119	120
diam_43_bo	0.68	8.16	1.90	0.06	1.71	12.51	1.58	1.52	1.53	(90 –	116)	1.50	125	116
diam_44_ch	12.40	5.79	2.18	–	11.16	31.54		(1.40 –	1.70)	(104 –	123)			
diam_44_bo	37.12	18.09	1.72	–	16.71	73.64		(1.39 –	2.10)	(90 –	126)			

Note. Crystalline and noncrystalline models are separated by a empty line. C…C, in Å, shows short interatomic distances between layers or corresponding bond distances created after compression. C12 are bond distances between independent carbons C1 and C2 or prior independent carbons. C11 are bond distances between pyramidal Csp^2 or prior pyramidal Csp^2. C22 are bond distances between planar Csp^2 or prior planar Csp^2. α_{op} are bond angles opposite to C1–C1 or C2–C2 bonds, like C2–C1–C2 or C1–C2–C1. α_{con} are for contiguous bond angles, like C1–C1–C2 or C2–C2–C1. For some less symmetric structures, averages or ranges (d_1-d_2) for bond lengths and angles are shown. Same energy calculations for referenced crystal structures are shown for comparison.

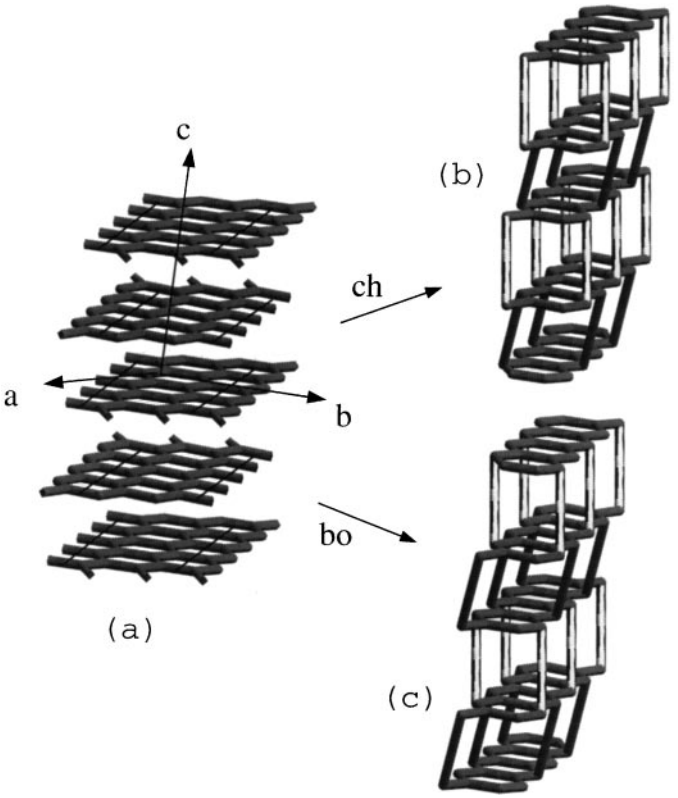

FIG. 2. (a) Layers of conventional graphite along the *c*-axis. The thin lines cross the breaking bonds, and the arrows are the directions of hexagonal cell axes. (b) Mechanism of transition from conventional graphite to graphite bilayers, where benzene is deformed to chair (ch). (c) Transition to graphite bilayers, where benzene is deformed to boat (bo).

pendent atoms included in this cell did not give significant variations in the atomic positions, which confirmed more *Cmma* as the best space group. These tests were also done for the rest of the models in Table 1, confirming in all cases the proposed space groups. The stacking of bilayers with boat conformations is described in a cell *Cmmm* with the structure gra_crbl33_bo shown in Fig. 3c. In both graphite bilayers, the rings of eight carbons are perpendicular to the *a*-axis, while the six-membered rings are perpendicular to the *b*-axis. Bilayer planes are parallel to the 10-carbon rings and stack along the *c*-axis. One bilayer of gra_crbl33_bo resembles one of the mentioned models proposed in the literature (18). On the other hand, the geometry of crystalline bilayers described in Table 2 are very close to the above mentioned noncrystalline fragments gra_bl_chair and gra_bl_boat, showing that these *materials* could be better described as crystals. However, the noncrystalline models are optimized without crystal constraints, hence approaching more (about 20% lower energy) to the optimal geometry.

At this point, we propose two different mechanisms (see Fig. 1) to follow the transition toward diamond. In the first (I), a compression along the new *c*-axis (see Fig. 3a) would approach bilayers in such a way that close pyramidal Csp^2 would bond, changing their hybridization to Csp^3. Thus, diamond structures with the mixture $1Csp^3:1Csp^2$ are formed, which can be proposed to describe some of the experimental phases referenced above (4–11). Figure 4a shows diam_cr43_ch (43 means the 4-connection and 3-connection of the two independent carbons), which come from gra_crbl33_ch. Figure 4b shows diam_cr43_bo, which come from gra_crbl33_bo, and forms four-membered rings. If we generate now $3 \times 3 \times 3 = 27$ cells of both diam_ structures, which makes two clusters of ~500 carbons, and optimize each cluster without crystal restrictions, they deform slightly giving the clusters diam_43_ch and diam_43_bo, described in Table 2, which confirms the probable crystallinity of these phases.

In the second mechanism (II) of the transition toward diamond (see Fig. 1), we compress graphite gra_crbl33_ch and gra_crbl33_bo along bilayer planes. In this way, two planar C2, opposite in the 10-carbon rings (see Figs. 3b or 3c), approach each other and bond (by changing their hybridization to Csp^3) forming two six-carbon rings. Thus, new structures of graphite diamond-like gra_crbl43_ch and gra_crbl43_bo are formed: the first *Pcca* (where axes' directions changed with respect to the *Cmma* structure: $a = b$(old), $b = c$(old), and $c = a$(old)) and the second *Pban* (conserving the same axes orientation as in *Cmmm*). Figures 5a and 5b show one bilayer of both structures (with rings of only six and eight carbons) that we also propose as interphases between graphite and diamond (4–11). It is interesting that orthorhombic gra_crbl43_ch structure presents a pseudo three-fold axis, which becomes real three-fold after the next compression step toward a cubic phase (see below). The two gra_crbl43 crystalline bilayers were extended with 6×6 translations on their plane, forming bilayer clusters of 600 carbons and, after a noncrystalline optimization, we got the nonplanar bilayers gra_bl43_ch and gra_bl43_bo. The significant nonplanarity of these clusters suggests that these structures can be better described as noncrystals. Hence, the stacking of these *flakes* could also model those materials found of low crystallinity with mixing of Csp^3 and Csp^2 (4–11).

Finally, crystalline bilayers of gra_crbl43_ch and gra_crbl43_bo can be approached in between by compression perpendicular to the layers, then close Csp^2 of neighbor bilayers would bond forming modified diamonds with all carbons sp^3. As a result, gra_crbl43_bo changes to diam_cr44_bo (with both independent carbons sp^3), which is the *Pban* structure shown in Fig. 6. This structure could also be derived from diam_cr43_bo by bonding opposite Csp^2 in C_{10} rings (see also Fig. 4b), both being the unique diamonds we found with C_4 rings. The structure diam_44_bo of Table 2 is the optimized noncrystalline cluster of 470 atoms. However, when by similar compression, we

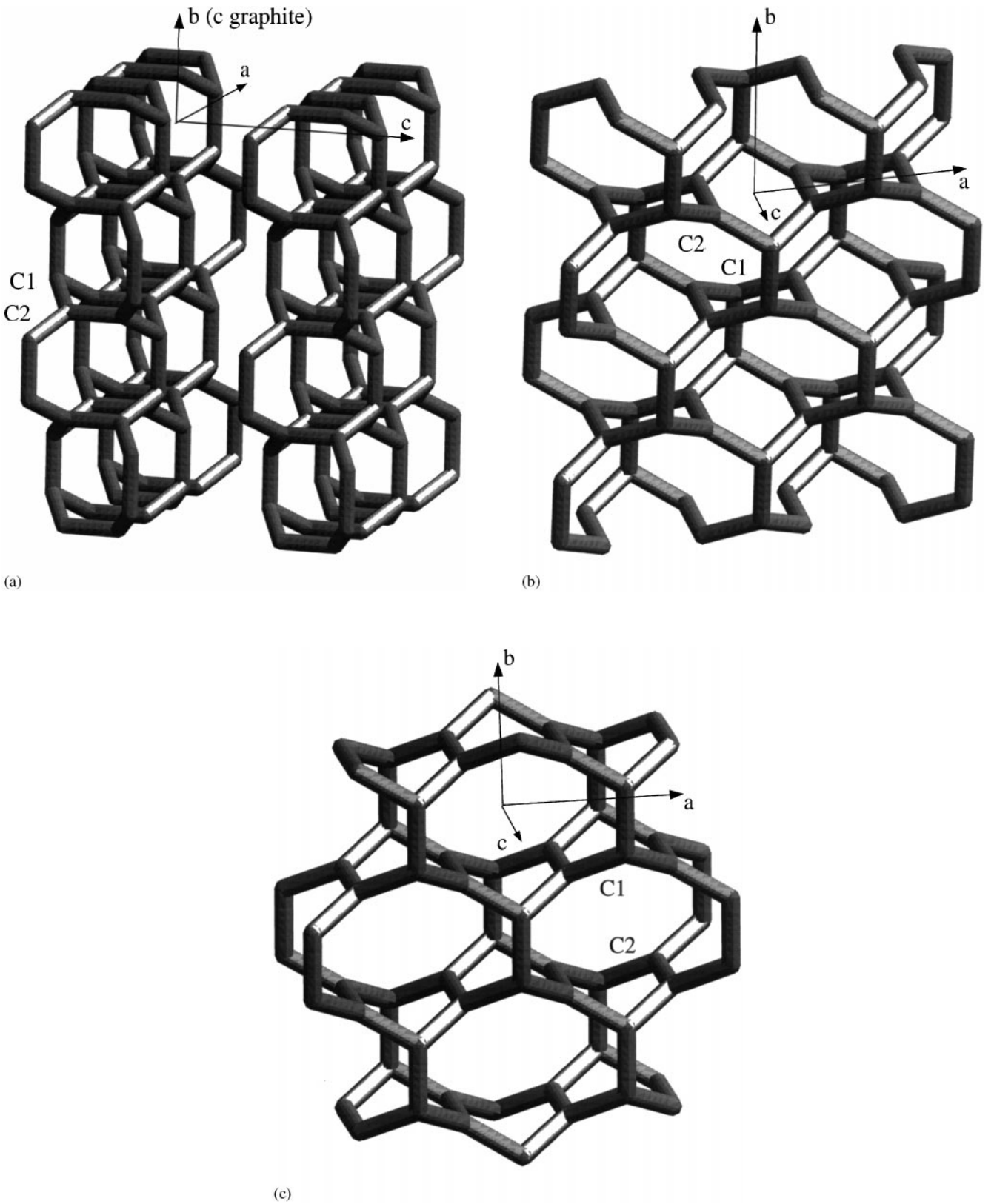

FIG. 3. (a) Two bilayers of gra_crbl33_ch viewed almost perpendicular to the 8-carbon-rings. (b) One bilayer of gra_crbl33_ch viewed almost perpendicular to the 10-carbon-rings. (c) One bilayer of gra_crbl33_bo viewed almost perpendicular to the 10-carbon-rings. The arrows indicate the directions of the cell axes in the *Cmma* or *Cmmm* crystals. The two independent sp^2 carbons C1 (pyramidal) and C2 (planar) are also indicated.

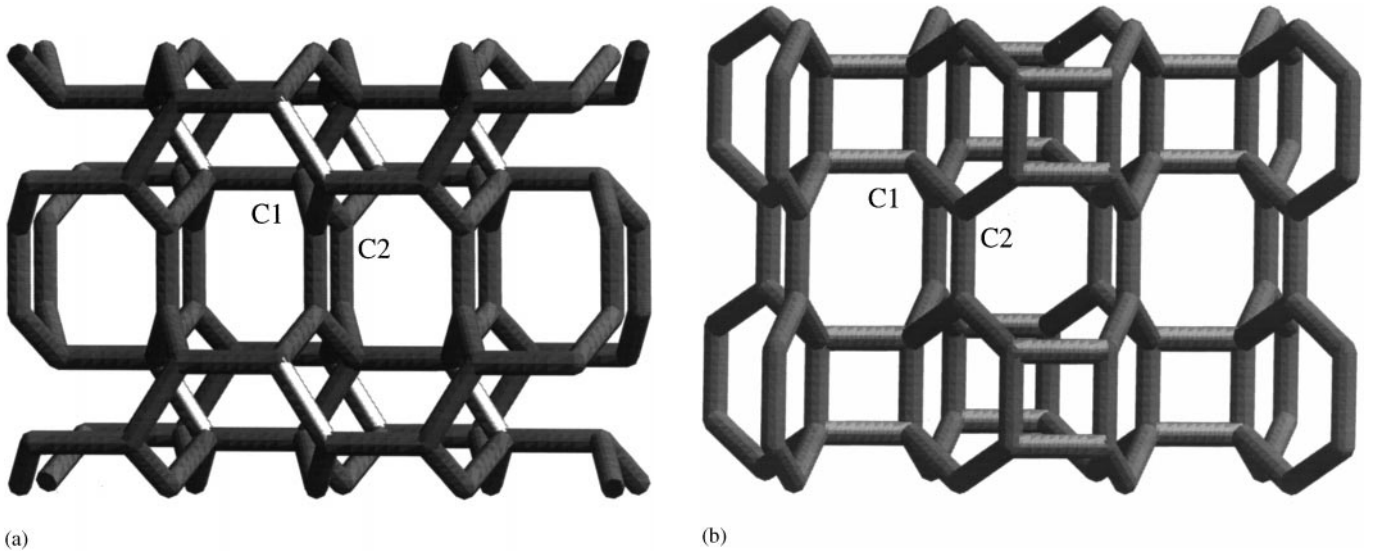

FIG. 4. (a) A fragment of diam_cr43_ch viewed almost perpendicular to the 8-carbon-rings. (b) A fragment of diam_cr43_bo viewed almost perpendicular to the 8-carbon-rings, showing the C_4 rings. The two independent carbons C1 (sp^3, tetrahedral) and C2 (sp^2, planar) are indicated.

approach bilayers of graphite gra_crbl43_ch, something unexpected happens, as this time the orthorhombic *Pbca* structure, with two independent carbons, is reordered into a new cubic *Ia*-3 structure diam_cr44_ch. This structure has only one independent carbon in the special position 16.c. (x,x,x) $x \sim 1/6$ (see Table 1), and it is shown in Fig. 7a. The structure could also be derived from diam_cr43_ch by bonding opposite Csp^2 in C_{10} rings (see also Fig. 4a). Figure 7b is a characteristic moiety of the *Ia*-3 structure, showing its six twist-boats six-member rings around a three-fold axis. By cutting bond BC and bonding D and E, we get a 3-boat plus 2-chair moiety characteristic of the hexagonal diamond, which is represented in Fig. 7c. This suggests a possible transition toward a real hexagonal diamond represented by a curved line in Fig. 1. The above transition can be made by computer but it is interesting to produce it manually on a plastic model by building the model of Fig. 7b and rebuilding it to Fig. 7c as described before. Then, one

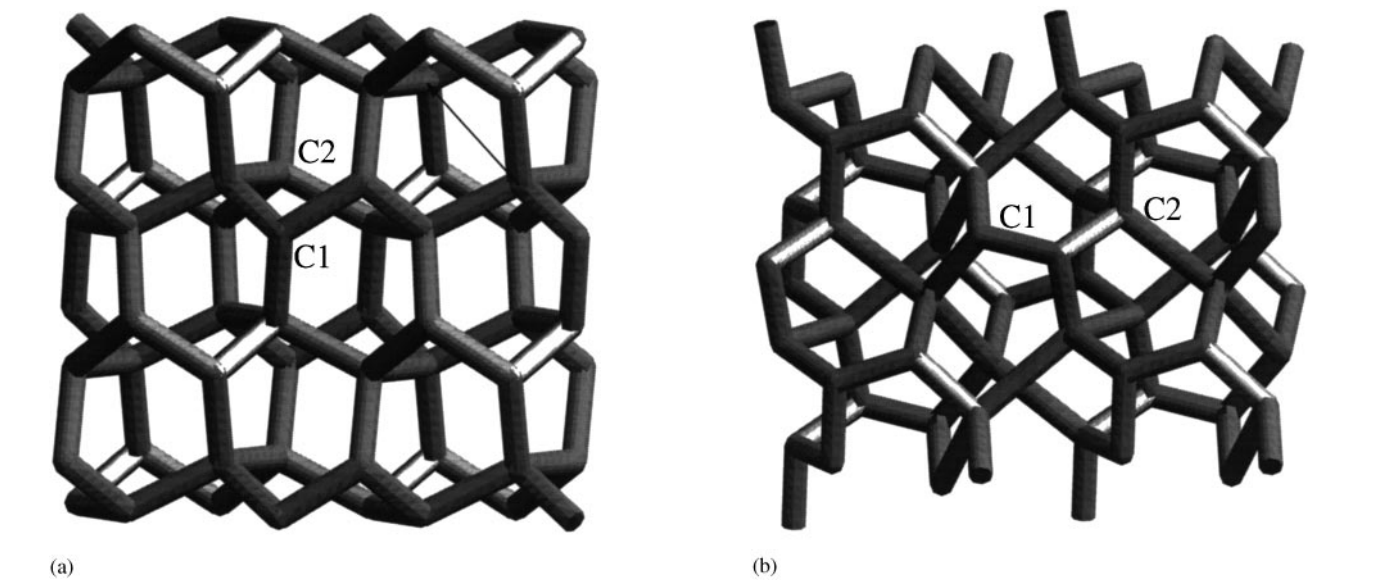

FIG. 5. (a) One bilayer of gra_crbl43_ch viewed almost perpendicular to both 6-carbon-rings originated by compression of one old 10-carbon-ring. The arrow indicates a pseudo three-fold axis generated after this compression. (b) The same for gra_crbl43_bo. The two independent carbons C1 (sp^2, pyramidal) and C2 (sp^3, tetrahedral) are indicated.

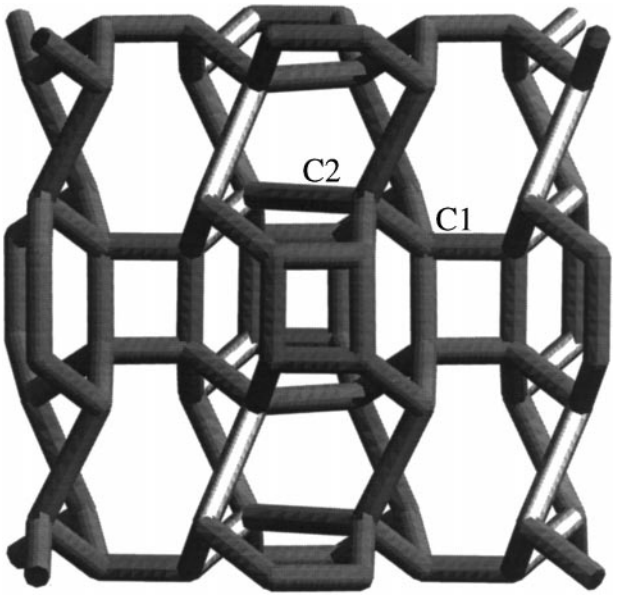

FIG. 6. A fragment of diam_cr44_bo showing the C_4 rings. Both independent carbons are tetrahedral sp^3.

can feel in the hands the strain of the structure relax, which would correspond to $\Delta E = 34$ Kcal/mol.at, as it is shown in Table 2. In fact, it is reported (20) that graphite changes to a hexagonal diamond by pressure of 130 Kbar and 1000°C, causing contraction of the graphite interlayer distance of 3.35 to a $\frac{1}{2}$4.12 Å distance in the diamond. The hexagonal *c*-axis of graphite is almost the vertical direction of Fig. 7, which is perpendicular to the twist-boat BCE of the *Ia*-3 structure (b); however, this direction is not well defined for the hexagonal diamond (c). Unfortunately, modification of

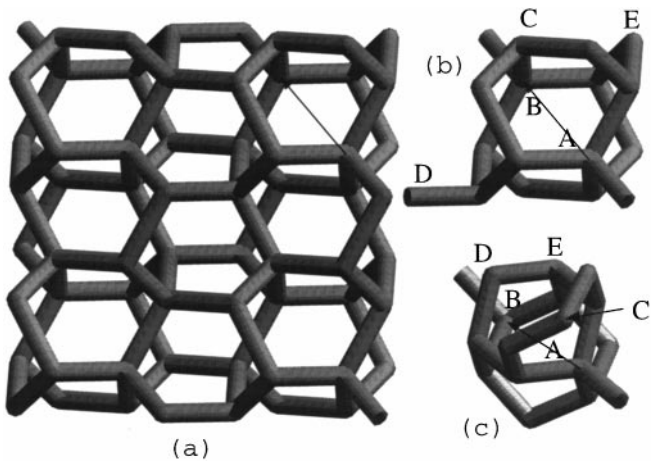

FIG. 7. (a) A fragment of the cubic *Ia*-3 structure diam_cr44_ch, showing the crystallographic three-fold-axis by an arrow. (b) The characteristic moiety of diam_cr44_ch, showing the six twist-boats around the three-fold-axis AB. When bond BC breaks and D bonds to E a hexagonal diamond is formed. (c) The resulting structure, which is indeed the characteristic moiety of a hexagonal diamond.

diam_cr44_ch to a cubic diamond seems to be more difficult. A fragment of 468 atoms of diam_cr44_ch was optimized as a noncrystalline cluster, with minor atomic displacements, giving the structure diam_44_ch shown in Table 2.

The *Ia*-3 structure of diam_cr44_ch, is just that proposed (3) as a better alternative structure (BC-8) for supercubane C8 (see Table 1). The main difference between both structures is that we optimized ours by taking into account VDW terms, which do not allow the compression of the intramolecular A…B distance (Fig. 7b), along the three-fold axis, below 2.58 Å as compared with that of 2.18 Å reported for the BC-8 carbon. If we optimize our structure without VDW terms (see diam_cr44_ch* in Table 1), this distance becomes 2.32 Å, with $a = 4.261$ Å and $d = 4.124\ \mathrm{gcm}^{-3}$, which is close to the values reported originally for supercubane (2), as it shows in Table 1. Geometry and energies of these structures are in Table 2.

Synthetic polycrystalline X-ray diffraction for all crystalline models of Table 1 have been compared with the observed peaks corresponding to reported (8) experimental phases between graphite and diamond. We found that graphite-bilayer models could contribute, especially with their biggest peaks of $5.6 < d < 6$ Å, to some evaporated carbon phases with $d_{\mathrm{obs}} = 5.24$ Å, which cannot be found in graphite or diamond where the largest spacings are observed at 3.34 Å and from 2.05 to 2.18 Å, respectively. The model diam_cr43_bo, with its biggest peak of 3.66 Å, and some other close to 2 Å, could contribute to another evaporated carbon phase and also to that found by pyrolysis of methane (8). And finally, diam_cr44_bo and diam_cr44_ch could contribute with their biggest peaks of $1.8 < d < 2.0$ Å to the phase obtained by glow discharge in C2H2 ($d = 2.0$ and 1.1 Å) (8).

CONCLUSIONS

The genealogical tree represented in Fig. 1 shows two principal routes of transition between graphite and diamond: the first forming intermediate structures containing 6-carbon-rings with chair conformation and the second containing 6-carbon-rings with boat conformation. There are some branches including different possible intermediate structures between graphite and diamond, where links between crystalline phases imply compression of the above structure toward the one below. In order of increasing density, we have graphite bilayers made of sp^2 carbons (one planar and the other trigonal); graphite bilayers made of mixed Csp^2 and Csp^3 in a 1:1 ratio; diamonds also with that combination of Csp^2:Csp^3; and modified diamonds made of just Csp^3. One of the latter diamonds is cubic and can be modified to a conventional hexagonal diamond. Although these are speculative structures, comparison of their molecular mechanic energies with the ones of conventional

graphite and diamond measures their relative stability. Table 2 also shows the geometrical deviation of each model from the optimal expected (but unattainable by optimization) one, which would have conventional bond lengths and bond angles between Csp^2 and Csp^3. It is significant that some of the crystalline models account for the principal XR peaks observed in experimental phases between graphite and diamond.

It is interesting to note the possible host character of the proposed carbon models, due to their large structural voids, which can be observed in the figures shown in this work.

Although all proposed structures are orthorhombic, one of the transition branches ends in a Csp^3 diamond with a cubic *Ia*-3 structure, which we found was coincident with the structure proposed before for supercubane C8 (3). In fact the original deformation of conventional graphite toward bilayer graphite implies a pseudo-cubic structure where carbons are 6 of the 12 corners of a regular icosahedron, forming a chair or a boat ring and building part of a *Pm*-3 structure of the A15-type (21). Finally, the structures of graphite bilayers could be compared with those of black phosphorus or those of α-As, Sb, or Bi, both with three connected atoms forming layers (1).

ACKNOWLEDGMENTS

I thank Felix H. Cano for helpful discussions and manuscript revision. This work was supported by the Comisión Interministerial de Ciencia y Tecnología (CICT) Grant PB98-0001-C03-02.

REFERENCES

1. B. K. Vainshtein, V. M. Fridkin, and V. L. Indenbom, "Modern Crystallography II, Structure of Crystals," p. 133. Springer-Verlag, Berlin, 1982.
2. N. N. Natyushenko, V. E. Strel'nitskii, and V. A. Gusev, *Cristallografiya* **26,** 484 (1981).
3. R. L. Johnston and R. Hoffmann, *J. Am. Chem. Soc.* **111,** 810 (1989).
4. R. C. De Vries, *Annu. Rev. Mater. Sci.* **17,** 161 (1987).
5. J. C. Angus and C. C. Hayman, *Science* **241,** 913 (1988).
6. R. H. Jarman, G. J. Ray, R. W. Standley, and G. W. Zajac, *Appl. Phys. Lett.* **49,** 1065 (1986).
7. N. Savvides, *J. Appl. Phys.* **58,** 518 (1985); **59,** 4133 (1986).
8. D. A. Anderson, *Philos. Mag.* **35,** 17 (1977).
9. Z. Li, L. Wang, T. Suzuki, A. Argoitia, P. Pirouz, and C. Angus, *J. Appl. Phys.* **73,** 711 (1993).
10. F. P. Bundy, *J. Chem. Phys.* **38,** 631 (1963).
11. W. C. Saslaw and J. E. Gaustad, *Nature* **221,** 160 (1969).
12. F. Diederich and Y. Rubin, *Angew. Chem.* **31**(9), 1101 (1992).
13. R. Hoffmann, T. Hughbanks, M. Kertész, and P. H. Bird, *J. Am. Chem. Soc.* **105,** 4831 (1983).
14. J. Elguero, C. Foces-Foces, and A. L. Llamas-Saiz, *Bull. Soc. Chim. Belg.* **101,** 795 (1992).
15. R. H. Baughman and H. Eckhardt, *J. Chem. Phys.* **87,** 6687 (1987).
16. H. Terrones, J. Fayos, and J. L. Aragon, *Acta Metall. Mater.* **42,** 2687 (1994).
17. K. M. Merz, Jr., R. Hoffmann, and A. T. Balaban, *J. Am. Chem. Soc.* **109,** 6742 (1987).
18. H. R. Karfunkel and T. Dressler, *J. Am. Chem. Soc.* **114,** 2285 (1992).
19. "CERIUS Version 3.2. Molecular Simulation," St. Johns's Innovation Centre, Cambridge, UK, 1993.
20. F. P. Bundy and J. S. Kasper, *J. Chem. Phys.* **46,** 3437 (1967).
21. J. Fayos, *J. Solid State Chem.* **119,** 364 (1995).